Environmental Science & Technology

Article

pubs.acs.org/est

Effect of Humic Acid on the Removal of Chromium(VI) and the Production of Solids in Iron Electrocoagulation

Chao Pan,[†] Lyndsay D. Troyer,[‡] Peng Liao,[§] Jeffrey G. Catalano,[‡] Wenlu Li,[†] and Daniel E. Giammar*[,†]

[†]Department of Energy, Environmental and Chemical Engineering and [‡]Department of Earth and Planetary Sciences, Washington University, St. Louis, Missouri 63130, United States

[§]School of Environmental Science and Engineering, Southern University of Science and Technology, Shenzhen Shi, Guangdong Sheng 518055, P. R. China

Supporting Information

ABSTRACT: Iron-based electrocoagulation can be highly effective for Cr(VI) removal from water supplies. However, the presence of humic acid (HA) inhibited the rate of Cr(VI) removal in electrocoagulation, with the greatest decreases in Cr(VI) removal rate at higher pH. This inhibition was probably due to the formation of Fe(II) complexes with HA that are more rapidly oxidized than uncomplexed Fe(II) by dissolved oxygen, making less Fe(II) available for reduction of Cr(VI). Close association of Fe(III), Cr(III), and HA in the solid products formed during electrocoagulation influenced the fate of both Cr(III) and HA. At pH 8, the solid products were colloids (1−200 nm) with Cr(III) and HA concentrations in the filtered fraction being quite high, while at pH 6 these concentrations were low due to aggregation of small particles. X-ray diffraction and X-ray absorption fine structure spectroscopy indicated that the iron oxides produced were a mixture of lepidocrocite and ferrihydrite, with the proportion of ferrihydrite increasing in the presence of HA. Cr(VI) was completely reduced to Cr(III) in electrocoagulation, and the coordination environment of the Cr(III) in the solids was similar regardless of the humic acid loading, pH, and dissolved oxygen level.

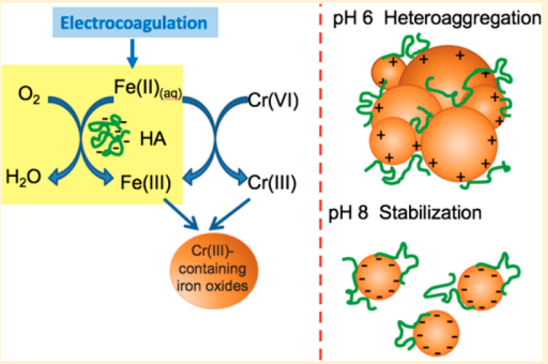

INTRODUCTION

Hexavalent chromium [Cr(VI)] is a toxic and carcinogenic metal found in groundwater and surface waters as a result of human activities and natural processes. A common Cr(VI) treatment technique involves Cr(VI) reduction to Cr(III) by Fe(II) and the subsequent association of Cr(III) with the produced Fe(III) (oxy)hydroxide solids.[1,2] The Cr(III) can either adsorb to or be structurally incorporated into the iron oxide by co-precipitation to form a Fe(III)−Cr(III) (oxy)-hydroxide solid solution.[3] Iron-based electrocoagulation (EC), where Fe(II) is produced from the iron anode, can lower the Cr(VI) concentrations to levels well below the 10 μg/L drinking water standard recently established in California.[4] In our recent work on electrocoagulation, the dynamics of Cr(VI) removal could be described by a model that incorporates Fe(II) release from the anode and heterogeneous and homogeneous reduction of Cr(VI) by Fe(II). The Fe- and Cr-containing EC product was found to catalyze that Cr(VI) reduction by adsorbed Fe(II). Iron electrocoagulation is also known to destabilize and remove natural organic matter (NOM, chiefly humic substances) by charge neutralization and sweep flocculation.[5,6] However, the influence of NOM on the extent and rate of Cr(VI) removal and the structure of the iron- and chromium-containing solids was not determined in the previous work.

Iron undergoes significant interactions with humic substances in the dissolved and particulate phases. Humic substances are complex organic macromolecules that are ubiquitous in water, soil, and sediments.[7] The concentration of humic substances in groundwater can be as high as 70 mg/L as dissolved organic carbon (DOC), whereas the DOC concentration in surface waters can be as high as 100 mg/L with an average concentration of 5 mg/L.[8−10] Humic substances can be in soluble (defined as diameter less than 1 nm) or colloidal forms (1 to 200 nm)[11] depending on solution conditions. Anionic functional groups, primarily carboxylic and phenolic groups, of humic substances introduce negative charges and have a strong affinity for positively charged mineral surfaces or metal cations.[9,12−14] NOM can become associated with iron oxides by adsorbing to already existing Fe oxides,[15,16] but it can also become associated with iron oxides during the initial formation of iron oxides. The precipitation of Fe(III) phases and immediate adsorption of NOM to the newly formed hydrous oxides and precipitation of NOM by monomeric or polymeric Fe species are parallel processes that have been

Received: January 19, 2017
Revised: April 14, 2017
Accepted: May 11, 2017

DOI: 10.1021/acs.est.7b00371
Environ. Sci. Technol. XXXX, XXX, XXX−XXX

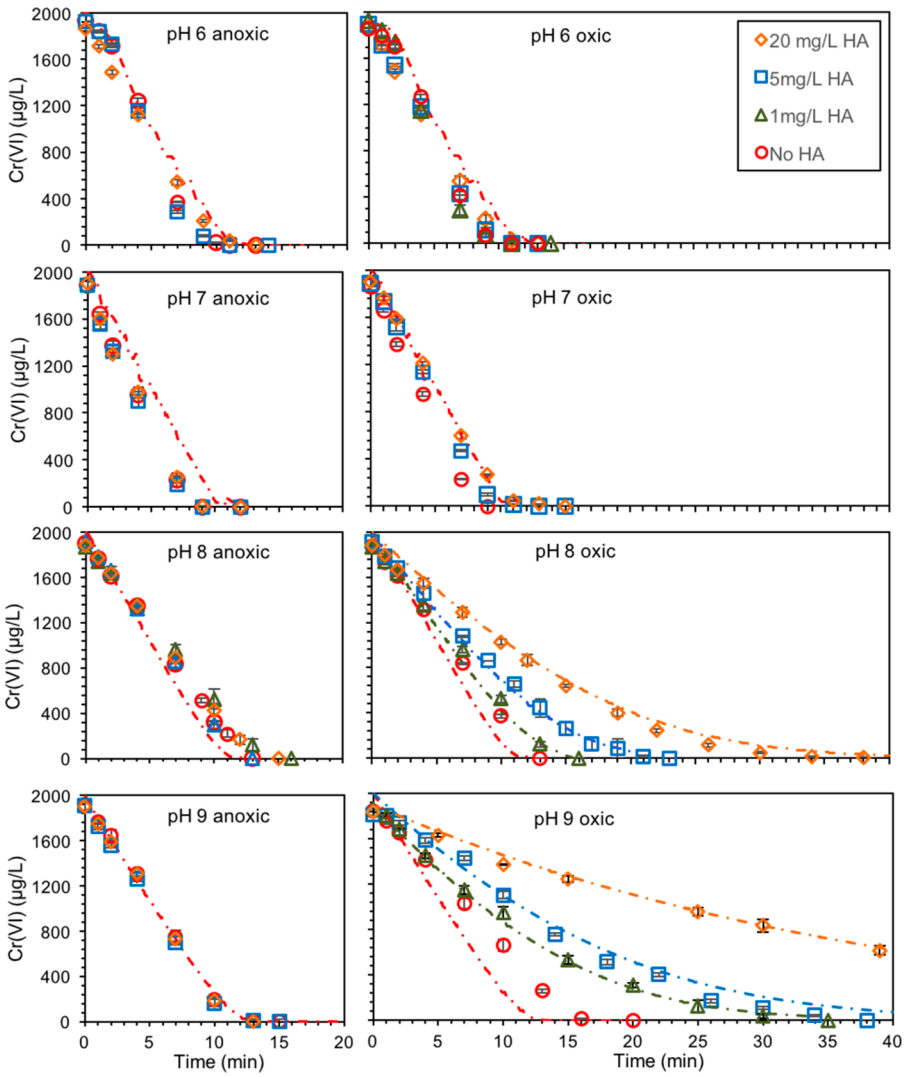

Figure 1. Influence of humic acid on Cr(VI) removal from pH 6 to pH 9 at oxic and anoxic conditions. The dashed lines correspond to simulations done according to the humic acid concentration present (Cr(VI) concentration derived from eq 1). Humic acid concentrations are expressed as mg C/L. Conditions: $[Cr(VI)]_0$ = 2 mg/L, U = 4 V, I = 37 mA, 2 mM MES for pH 6.0, 5 mM HEPES for pH 7.0 and 8.0, 5 mM CHES for pH 9, and conductivity = 460 μS/cm.

referred to as co-precipitation.[17,18] Co-precipitation of NOM with Fe is common in environments where Fe hydrolysis occurs due to changes in pH or redox potential.[19] Lalonde et al. estimated that around 21.5% of organic carbon is co-precipitated or adsorbed to reactive iron oxide phases in sediments across a wide range of depositional environments. Simple adsorption of organic matter on reactive iron oxide surfaces accounts for little uptake compared with co-precipitation and/or chelation of organic compounds with iron oxides.[13] In addition to the stabilization of NOM by association with iron oxides,[5,6] co-precipitation is also known to alter the particle size and structural order of the newly formed oxyhydroxides.[20,21] Eusterhues et al. found that even a small amount of NOM significantly affects crystal growth, leading to smaller ferrihydrite crystals, increased lattice spacing, and greater distortion of Fe(III) octahedra.

Besides interacting with metal oxides, humic substances also bind soluble metal ions, which is important for the speciation, transport, and toxicity of these trace metals.[22−24] Cr(III) binds to Suwannee River fulvic acid (SRFA) as a monomeric Cr(III)−SRFA complex at pH < 5, but it binds as polynuclear Cr(III)−SRFA at higher pH.[23] However, fewer studies have examined the chemistry of HA in systems containing both Cr(III) and Fe(III).[25,26]

Dissolved organic matter can affect the rate of Fe(II) oxidation by dissolved oxygen.[27−30] A variety of iron(II)-binding ligands and humic acids were found to decrease the rate of iron(II) oxidation.[28] However, it has been noted that back reduction of Fe(III) species by catechol-type ligands may have decreased their observed oxidation rate.[31] In contrast, Liang et al.[32] found that DOM can accelerate the iron(II) oxidation rate under some conditions. This study and another postulated that in the presence of DOM net oxidation is the result of two competing pathways, DOM−iron(II) complexation followed by oxidation of the complex and oxidation of inorganic iron(II) species.[32,33] In addition to the influence of complexed HA on Fe(II) oxidation, HA could also directly influence Cr(VI) reduction by Fe(II) at suboxic conditions. Cr(VI) reduction by Fe(II) was reported to be accelerated in the presence of different organic ligands, and the acceleration extent is dependent on pH.[34−36]

DOI: 10.1021/acs.est.7b00371
Environ. Sci. Technol. XXXX, XXX, XXX−XXX

The objectives of this study were to evaluate the effect of HA on the process of Cr(VI) removal by Fe electrocoagulation, including its influence on the dynamics of Cr(VI) reduction, the colloidal stability of solids produced from electrocoagulation, and the coordination environments of chromium and iron in these solid products. We chose humic acid as a representative NOM to evaluate its effects on Cr(VI) removal by electrocoagulation. Humic acid might affect the process by inhibiting or accelerating the rates of Fe(II) oxidation by dissolved oxygen and Cr(VI) reduction by Fe(II), reducing Cr(VI) with specific ligands, competitively adsorbing onto reactive sites of iron oxides, adjusting or even reversing the electrostatic charge of mineral surfaces, and forming colloids composed of HA, Fe(III), and Cr(III).

MATERIAL AND METHODS

Materials. Chemicals used were analytical reagents of high purity. Ultrapure water (resistivity >18.2 MΩ-cm) was used for the experiments. Glass volumetric flasks and 1 L polypropylene reaction vessels were cleaned with 10% HCl and rinsed several times with ultrapure water before use. A Cr(VI) stock solution (0.1 g/L, 1.923 mM) was prepared from $K_2Cr_2O_7$. Control of ionic strength was achieved by addition from a 1 M $NaNO_3$ stock solution. At pH 6, 1 mM MES (2-(*N*-morpholino)-ethanesulfonic acid) (Fisher Scientific) was used, 2 mM HEPES (4-(2-hydroxyethyl)-1-piperazineethanesulfonic acid) (≥99.5%, Sigma-Aldrich) was used at pH 7 and 8, and 2 mM CHES (*N*-cyclohexyl-2-aminoethanesulfonic acid) (≥99.5%, Sigma-Aldrich) was used for experiments at pH 9. The pH buffers and their concentrations were chosen to minimize the possible formation of Fe(III) and Cr(III) complexes with the buffers.[37,38] MES, HEPES, and CHES are widely used for their minimal influences on metal complexation.[39−43] Commercial humic acid was chosen as a model for colloidal humic substances (Sigma-Aldrich). Sigma-Aldrich humic acid displays similar redox properties (midpoint potential and electron accepting capacity) as those of soil-derived humic acids,[44] and it has been used in numerous other studies.[26,45,46] The stock solution of HA was filtered through a 0.45 μm poly(ether sulfone) (PES) membrane (Millipore) under vacuum and stored in the dark at 4 °C before use.

Electrocoagulation Batch Experiments. The electrocoagulation reactor and procedure were the same as described in detail in our previous work.[4] Briefly, the electrocoagulation reactor consisted of two iron rods immersed in a 1 L solution with 2 mg/L (38.5 μM) initial Cr(VI) and 5 mM buffers. Sodium nitrate was added until the conductivity of the solution achieved 460 μS/cm. An electric potential of 4 V was applied to the rods with a direct current power supply, and the current was held constant at 37 mA. Anoxic experiments were performed in an anaerobic chamber (Coy Laboratory Products Inc., MI) with a secondary low temperature oxygen trap to achieve strictly anoxic conditions in the electrocoagulation reactor.[4,47] All of the EC experiments for Cr(VI) removal with different concentrations of HA were performed in duplicate with error bars representing standard deviation, as shown in Figure 1.

For each sampling event, a volume of suspension was drawn from the reactor. The suspensions for analyzing total iron and chromium were acidified directly after collection. The rest of the suspension in the syringe was filtered through a 0.22 μm poly(ether sulfone) (PES) membrane, and the filtrate was saved for analysis of dissolved iron, chromium, Cr(VI), Fe(II), and humic acid concentrations. The aliquots for Cr(VI), Fe(II), and HA were not acidified and measured immediately after being collected. Only the separate aliquots for ICP-MS measurements were preserved with 2% HNO_3.

Analysis. Cr(VI) concentrations in the samples were determined with the diphenyl carbazide (DPC) method by measuring the absorbance at 540 nm using a spectrophotometer (PerkinElmer-Lambda XLS).[48] Total dissolved Fe(II) concentrations were determined spectrophotometrically by the ferrozine method at a wavelength of 562 nm.[49] Total dissolved iron and total dissolved chromium (Cr(VI) and Cr(III) together) concentrations were measured by inductively coupled plasma mass spectrometry (ICP-MS) (PerkinElmer ELAN DRC II) analysis of filtered samples. In experiments without humic acid, dissolved Fe(II) concentrations were found to be equal to dissolved iron concentrations because Fe(III) has a very low solubility in the range of pH 6−9 that was studied. The organic carbon concentration of the humic acid stock solution was determined by a total organic carbon analyzer (TOC-L, Shidmadzu Scientific Instruments, Inc., MD). DOC concentrations of filtered samples were measured spectrophotometrically at 254 nm using a 1 cm quartz cell. To eliminate interference from Fe(III) in absorbance measurements for DOC determination, 0.05 mL of 5% hydroxylamine hydrochloride was added to each 1 mL sample and the absorbance was recorded until no further change occurred, indicating that all the Fe(III) had been reduced to noninterfering Fe(II).[50]

Soluble (<10 kDa), colloidal (10 kDa, 0.22 μm), and particulate (>0.22 μm) Cr, Fe, and HA were fractionated from samples by 10 kDa ultrafiltration and 0.22 μm filtration. Colloids in this study were defined as particles ranging from 10 kDa (roughly equal to 1−3 nm) to 0.22 μm (the initial filtration). Specifically, the colloidal samples were operationally isolated by the pore size of separating devices; i.e., filtered water samples (filtrates) were separated into permeates (<10 kDa, soluble phase) and retentates (10 kDa, 0.22 μm, concentrated colloidal phase) by ultrafiltration membranes (MF-Millipore) with nominal molecular weight cut-offs of 10 kDa.

The particle size distributions and zeta potential of electrocoagulation products were measured through dynamic light scattering (DLS) analysis (ZetaSizer Nano, Malvern Instruments, UK). For each sampling event, the suspension was taken from the electrocoagulation reactor and measured by DLS within 5 min. TEM samples were prepared by dropping approximately 30 μL of electrocoagulation suspension quickly onto 200 mesh carbon-coated copper grids (Ted Pella, Inc.) followed by immediate evaporation of the remaining water at room temperature under vacuum. TEM micrographs were taken with a transmission electron microscope under 120 kV (FEI Spirit G2). Solids for X-ray powder diffraction (XRD) were collected from suspensions after 30 min of electrocoagulation reaction. The suspensions were concentrated by centrifugation and then freeze-dried. XRD patterns of solid samples were collected using Cu Kα radiation (Bruker d8 Advance X-ray diffractometer).

Fe and Cr K-edge X-ray absorption fine structure (XAFS) spectra were collected on samples from electrocoagulation reactors after 30 min of reaction. Samples were vacuum-filtered onto mixed cellulose ester membranes (0.22 μm) and then sandwiched as wet pastes between Kapton film and sealed with Kapton tape. XANES spectra were collected at the Advanced Photon Source on beamlines 5-BM-D and 20-BM-B. 5-BM-D and 20-BM-B both employ a water-cooled Si (111) double-

DOI: 10.1021/acs.est.7b00371
Environ. Sci. Technol. XXXX, XXX, XXX−XXX

crystal monochromator; harmonic rejection is achieved through detuning the monochromator by 10−30% and beamline-specific mirror configurations.[51,52] Fluorescence-yield spectra were collected with a four-element energy-dispersive silicon drift detector at beamline 5-BM-D and were collected with a 13-element solid state Ge energy-dispersive detector at beamline 20-BM-B. Fe reference compounds included lepidocrocite and two-line ferrihydrite. Two-line ferrihydrite was synthesized by dissolving $Fe(NO_3)_3{\cdot}9H_2O$ in DI water and adding NaOH to bring the pH to 7. The suspension was then dialyzed to remove dissolved sodium and nitrate, and the cleaned suspension was freeze-dried.[53] Lepidocrocite was synthesized using previously described procedures.[53] Cr reference compounds of Fe(III)−Cr(III) co-precipitates were synthesized by first combining Fe(III) chloride and Cr(III) chloride stock solutions in varying ratios with a total concentration of 60 μM Fe and Cr with 10 mM NaCl as a background electrolyte. The solutions were then adjusted to pH 7 using NaOH and stirred for 2 days before being prepared by vacuum filtration in the same way as the samples. Fe and Cr spectra were processed in the Athena[54] interface to IFEFFIT.[55] Athena was also used for linear combination fitting of Fe extended X-ray absorption fine structure (EXAFS) spectra. Structural models of Cr EXAFS spectra were refined in SIXPack[56] using backscattering phase and amplitude functions generated from FEFF 7.02.[57,58]

Modeling the Dynamics of Cr(VI) Removal. Reaction kinetics considering Fe(II) generation in EC, Cr(VI) reduction by Fe(II), Fe(II) oxidation by dissolved oxygen (DO), and acceleration of Fe(II) oxidation by DO caused by HA were applied to simulate the dynamics of dissolved Cr(VI) and Fe(II) during electrocoagulation. The rates of change of Cr(VI) (eq 1) and Fe(II) (eq 2) during electrocoagulation can be written as

$$-\frac{d[Cr(VI)]}{dt} = k_{homo}[Cr(VI)]_{diss}[Fe(II)]_{diss} + k'_{hetero}[Fe(III)]_s[Cr(VI)]_{diss}[Fe(II)]_{diss} \quad (1)$$

$$-\frac{d[Fe(II)]}{dt} = 3k_{homo}[Cr(VI)]_{diss}[Fe(II)]_{diss} + 3k'_{hetero}[Fe(III)]_s[Cr(VI)]_{diss}[Fe(II)]_{diss} - k_2 + fk_{O_2}[Fe(II)]_{diss} \quad (2)$$

The definitions and values of the rate constants are summarized in Table S1. The development and initial parametrization of the model were described in our recent work on experiments in the absence of humic acid.[4] Briefly, eq 1 includes both homogeneous and heterogeneous reduction of Cr(VI). In eq 2, the four terms are included to track the fate of Fe(II) as it is affected by (i) homogeneous and (ii) heterogeneous reaction of Fe(II) with Cr(VI), (iii) Fe(II) production from the anode according to Faraday's law, and (iv) Fe(II) oxidation by dissolved oxygen. The terms of heterogeneous reactions are simplified under the assumption that any minor fraction of adsorbed Cr(VI) does not strongly affect the kinetics and that adsorbed Fe(II) is proportional to the dissolved Fe(II). In the presence of HA, the rate of Fe(II) oxidation by DO would increase and enhancing factors were used to represent the increasing extent. The enhancing factor of Fe(II) oxidation with different HA concentration (f) was an adjustable parameter that was used to fit the model output to the experimental data. Because the rest of the model had been previously developed from independently determined parameters, the enhancing factor was the only fitting parameter in the present study.

RESULTS AND DISCUSSION

Effect of Humic Acid on Cr(VI) Removal Rate in Electrocoagulation. Without the presence of oxygen, HA had no effect on the rate of Cr(VI) removal from pH 6 to pH 9 (Figure 1). Although HA was previously reported to accelerate Cr(VI) reduction by Fe(II),[34] this was not observed from pH 7 to pH 9 even without oxygen. The lack of an observable effect of HA at anoxic conditions suggests that Fe(II) generation from the anode in electrocoagulation was the rate-limiting step for Cr(VI) removal,[4] and the reduction of Cr(VI) by Fe(II) either with or without HA was much faster than Fe(II) production.

With oxygen present, HA inhibited Cr(VI) removal at the higher pH conditions studied (Figure 1). Humic acid has a high density of carboxylate functional groups that complex with both Fe(II) and Fe(III).[59] The strong complex with Fe(III) could drive down the free Fe(III) concentration and lower the reduction potential of the Fe(III)/Fe(II) half reaction; thus, Fe(II) could be more easily oxidized by dissolved oxygen.[60,61] In addition, the complexation of Fe(II) by carboxylate functional groups increases the rate of Fe(II) oxidation by O_2 compared to uncomplexed Fe(II).[29] Thus, Cr(VI) reduction by Fe(II) was inhibited as oxygen became a strong competitor with Cr(VI) to oxidize Fe(II)−HA complexes. The greater inhibition of Cr(VI) removal by HA at higher pH during electrocoagulation might be due to the pH dependence of the rate of the complexed Fe(II) oxidation by O_2. Figure S1 shows the influence of HA on the evolution of dissolved Fe(II) in electrocoagulation at oxic conditions without the presence of chromium. The enhancement of Fe(II) oxidation was not observed at pH 6 in electrocoagulation (Figure S1a), and the Fe(II) concentration with or without HA was similar to total iron (represented by Faraday's law, eq S1 in the Supporting Information). The Fe(II) oxidation by dissolved oxygen was too slow at pH 6 and could be negligible within the short time of electrocoagulation. At a higher pH of 7, it is easier to see the trend of Fe(II) oxidation acceleration in electrocoagulation (Figure S1b). At pH 8, no accelerating effect of HA on Fe(II) oxidation can be discerned because the rate was very fast even in the absence of HA (Figure S1c). Fe(II) was immediately oxidized once generated in electrocoagulation even without HA. This pH dependence of the HA-enhanced oxidation of Fe(II) by O_2 might be due to a greater abundance of deprotonated carboxyl groups that could complex Fe(II) better at higher pH.

We applied the model for the dynamics of Fe(II) and Cr(VI) during electrocoagulation at both oxic and anoxic conditions (eqs 1 and 2). For the processes with HA present, we increased the Fe(II) oxidation rate constant by changing the value of the enhancing factor f in the term of Fe(II) oxidation by DO (eq 2). The enhancing factors for Fe(II) oxidation, f, are summarized in Table S2. The enhancing factors necessary to fit the evolution of Cr(VI) during electrocoagulation increased with increasing pH and humic acid concentrations. At pH 7, it is hard to precisely determine the enhancing factors of different HA concentration as experimentally there is a slight enhancement of Fe(II) oxidation (Figure S1b) and inhibition of Cr(VI) removal (Figure 1) and at pH 6 there is no experimental

DOI: 10.1021/acs.est.7b00371
Environ. Sci. Technol. XXXX, XXX, XXX−XXX

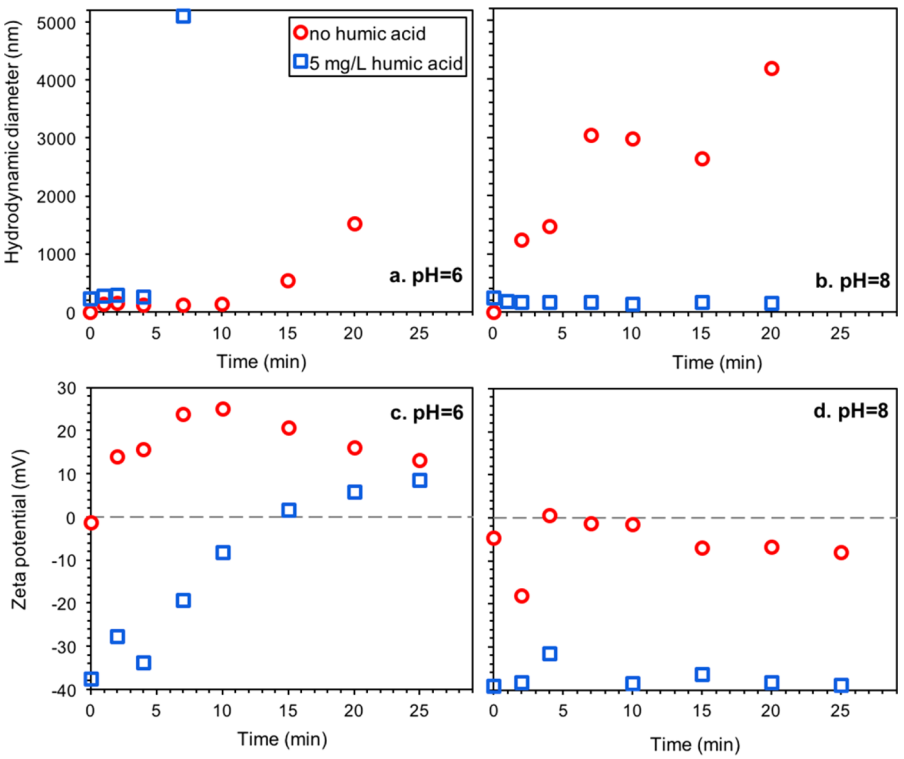

Figure 2. Hydrodynamic diameter at (a) pH 6 and (b) pH 8 and electrophoretic mobility of particles produced during electrocoagulation at (c) pH 6 and (d) pH 8 for conditions with (blue squares) and without (red circles) 5 mg/L HA; $Cr(VI)_0$ = 2 mg/L, U = 4 V, I = 0.037 A.

evidence for even a slight enhancing factor of Fe(II) oxidation by HA. In modeling the behavior at both pH 6 and 7, the enhancing factor could be set to 1 (i.e., no enhancement), and acceptable fits were achieved. Including any factor greater than 1 at pH 7 would actually have resulted in poorer fits. The evolution of the Fe(II) concentration during electrocoagulation calculated by the model is shown in Figure S2. According to the model output, HA would not influence the macroscopically observable Fe(II) concentration evolution even at oxic conditions from pH 6 to 9. This is because any HA enhancement of Fe(II) oxidation by dissolved oxygen is not apparent at pH 6, is very limited at pH 7, and is not observable at pH 8 and above because all Fe(II) is immediately oxidized once generated even without HA. In the model equations, it is assumed that all the Cr(VI) in EC solids is reduced to Cr(III) even in the presence of humic acid. This is consistent with the XANES spectroscopy results discussed below.

Effect of HA on the Formation of Colloidal Particles in Electrocoagulation. The overall performance of iron electrocoagulation and its integration with other unit operations in water treatment will depend on the coagulation of the particles produced in addition to the Cr(VI) removal just discussed. Humic acid enhanced coagulation−flocculation at pH 6, while it inhibited coagulation−flocculation at pH 8. Without HA, Fe−Cr solid particles produced from electrocoagulation are positively charged below pH 6.5 as determined from zeta potential measurement (pH_{pzc}= 6.5 in Figure S3). This pH dependence of surface charge is comparable to that reported by Wan et al., where the lepidocrocite produced in electrocoagulation had an isoelectric pH of about 7.0.[62] As a result, solid particles generated during electrocoagulation with no HA present had zeta potentials that were positive at pH 6 (Figure 2c) and negative at pH 8 (Figure 2d). Particle size measured by DLS provides information on the changes in the state of colloidal systems. Without HA at pH 6, electrostatically repulsive interactions predominantly reduced the collision efficiency of particles due to their positive charge. Iron oxide solids were colloids for the first 10 min and then aggregated into larger particles as more iron oxide particles were generated (Figure 2a). The humic acid influences the surface charge properties of electrocoagulation products, which govern particle−particle interactions. Since the produced amount of iron oxide is low at the beginning of EC process, the negatively charged HA adsorbs and thus neutralizes the positive charges on the iron oxide surface at pH 6 and gives the initial solids formed a net negative charge. In this process, the heteroaggregation between the HA and iron oxides was promoted due to favorable electrostatic attractions between oppositely charged particles.[63] With more output of positively charged iron oxides generated from EC, the surface charge of particles became less negative than 30 mV within 5 min, and eventually the surface charge was reversed at 15 min. The charge neutralization and reversal led to an unstable particle system in which aggregation occurred. As seen in Figure 2a for the case of 5 mg/L HA at pH 6, the aggregate size already exceeded 1 μm after 5 min. DLS does not give information on very large particles so we only showed the data up to 5 min.

Particles with zeta potentials more positive than +30 mV or more negative than −30 mV are normally considered stable.[64] Figure 2d shows the surface charge of EC products at pH 8 in the absence and presence of HA. Iron oxides generated in EC without HA are only slightly negatively charged at pH 8, and thus, aggregation to larger particles occurs easily. The particle size increased from 0 to 1000 nm in less than 1 min. In the presence of 5 mg/L HA at pH 8, the surface charge of solid particles generated during electrocoagulation is always negative (ca. −40 mV). Under this condition, the particle size is stable, ranging from 163 to 244 nm during the whole EC process. The

DOI: 10.1021/acs.est.7b00371
Environ. Sci. Technol. XXXX, XXX, XXX−XXX

stabilization of colloidal particles by HA at pH 8 (Figure 2b) can be ascribed to the enhanced electrosteric stabilization effect from adsorbed HA,[16] which increases the dispersion of the particles.

The stability of the particles in electrocoagulation greatly influences the fate of Cr(III). All Fe(II) and Cr(VI) are soluble as no Cr(VI) or Fe(II) were detected in large particles or colloids. All Cr(III), Fe(III), and HA were present in either colloids or larger suspended particles because of their negligible concentration detected in soluble filtrates after 10 kDa membrane ultrafiltration. Thus, the colloidal concentrations of Cr(III), Fe(III), and HA are the same as their concentrations in the samples filtered with 0.22 μm membranes, which are recorded in Figure S4. Figure 3 summarizes the fractions of the

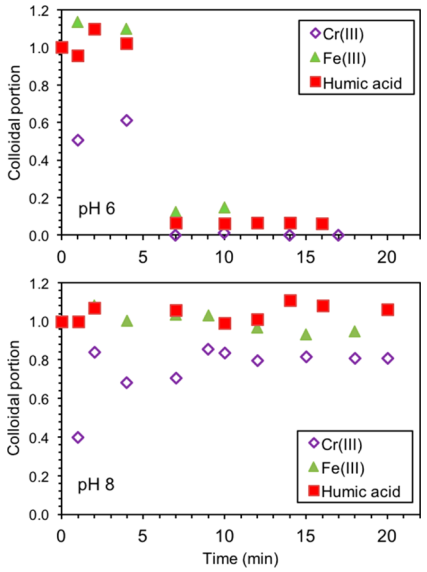

Figure 3. Colloid conditions of solids produced during electrocoagulation at pH 6 and pH 8. The colloidal portion is the concentration of colloidal Cr(III), Fe(III), and HA divided by the concentration of total Cr(III), Fe(III), and HA, respectively.

total amounts of Cr(III), Fe(III), and HA that are present as colloids following electrocoagulation. In the first 5 min at pH 6, when EC products with HA are small colloidal particles, the colloidal fractions of Cr(III), Fe(III), and HA concentrations are close to 1. However, after 5 min, the Cr(III), Fe(III), and HA aggregated and became larger particles. At pH 8, the negatively charged HA prevents the aggregation of particles, and the Cr(III), Fe(III), and HA were colloids at pH 8 over the entire duration of electrocoagulation. The consistent colloidal behaviors among Cr(III), Fe(III), and HA indicate their close associations during electrocoagulation.

HA removal during the electrocoagulation process is also important as NOM has been identified as a precursor to harmful disinfection byproduct (DBP) from upon contact with chlorine disinfectants.[65−68] It can be seen in Figure 3 that HA is present in stable colloids during electrocoagulation at high pH. However, HA could still be aggregated in EC with optimized operation conditions, e.g., increasing anodic Fe(II) dosage rate or dosage time. Many studies in recent years have reported that iron-electrocoagulation operations can be effective at removing natural organic matter.[5,6,69] The presence of divalent cations (Ca^{2+} and Mg^{2+}) might also introduce HA aggregation and subsequent removal by filtration.[70,71]

Characterization of Precipitates Produced during Electrocoagulation. XRD measurements (Figure 4) show

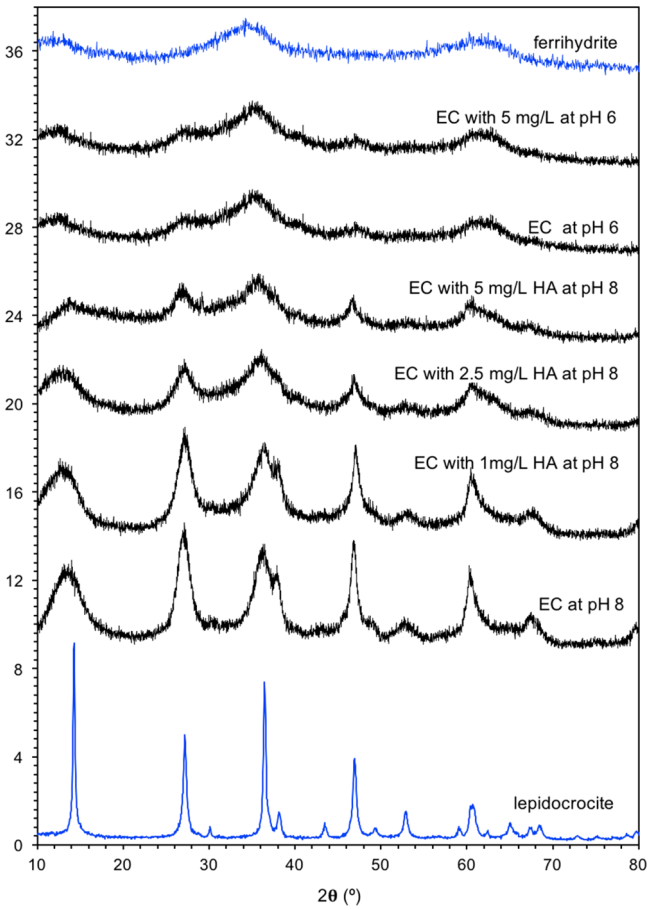

Figure 4. XRD patterns of iron oxides produced during electrocoagulation without chromium present at various conditions. For reference, the patterns of pure lepidocrocite and two-line ferrihydrite are included in XRD plots.

that both pH and the presence of HA affect the mineralogy of iron oxides produced during electrocoagulation. The patterns suggest that ferrihydrite dominates at pH 6, with nanocrystalline lepidocrocite also likely present, whereas lepidocrocite dominates at pH 8. The addition of HA has little apparent effect on the mineralogy at pH 6 but leads to a decrease in lepidocrocite coherent domain size (as indicated by the broadening of the XRD reflections) at pH 8. The higher concentrations of HA used may also increase the production of ferrihydrite at pH 8.

EXAFS spectroscopy (Figure 5) was used to quantify the iron mineralogy produced via electrocoagulation with and without HA and Cr(VI) because such quantification of nanocrystalline phases is not possible via XRD. All spectra were modeled via linear combination fitting using the spectra of lepidocrocite and ferrihydrite and the phases identified as being dominant components in XRD. Fitting confirms that in the absence of HA lepidocrocite is the sole mineral product of electrocoagulation at pH 8 but that ferrihydrite dominates at pH 6, with a minor lepidocrocite component present (Table 1). The addition of HA, Cr(VI), or both species favors an increased formation of ferrihydrite at pH 8. In contrast, at pH 6 neither HA nor Cr(VI) appreciably affects the ratio of

DOI: 10.1021/acs.est.7b00371
Environ. Sci. Technol. XXXX, XXX, XXX−XXX

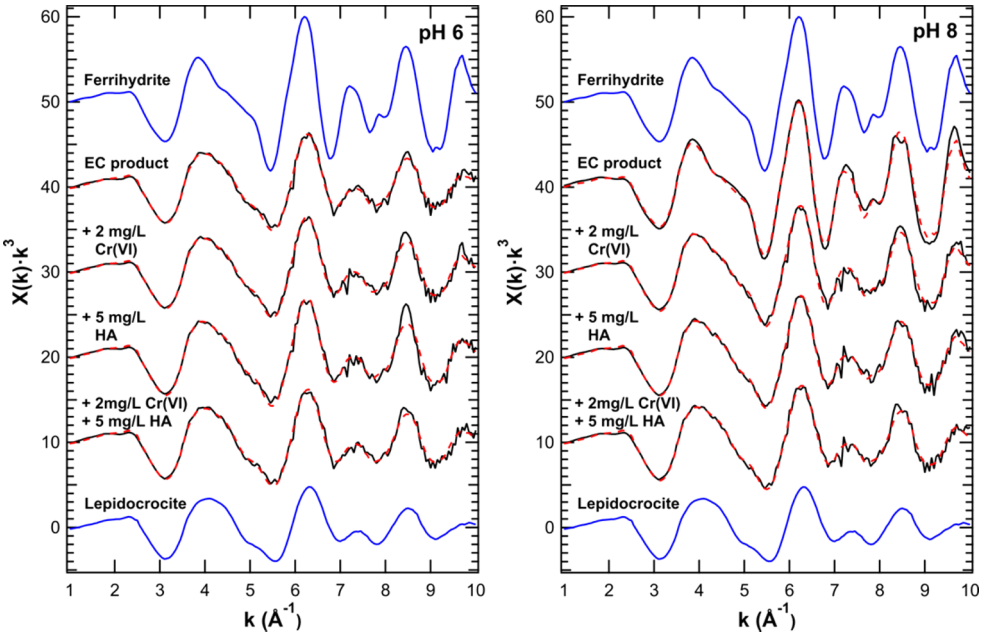

Figure 5. Fe K-edge EXAFS spectra of iron oxides produced during electrocoagulation in the presence and absence of chromium at various conditions. For reference, the patterns of pure lepidocrocite and two-line ferrihydrite are included in the EXAFS plots.

Table 1. Fe K-Edge EXAFS Linear Combination Fitting Results for Solids Generated in the Electrocoagulation Reactor

			percent component		
Cr (mg/L)	HA (mg/L)	pH	lepidocrocite	two-line ferrihydrite	component sum
		6	20 ± 1	80 ± 2	1.10
2		6	27 ± 2	73 ± 3	1.09
	5	6	31 ± 2	69 ± 3	1.12
2	5	6	17 ± 1	83 ± 2	1.13
		8	100	0	1.00
2		8	48 ± 2	52 ± 3	1.10
	5	8	37 ± 2	63 ± 3	1.11
2	5	8	23 ± 1	77 ± 3	1.15

ferrihydrite to lepidocrocite, with the former dominating under all conditions studied.

The influence of HA and Cr(VI) on the Fe(III) solids produced at pH 8 likely results from their effect on Fe(III) nucleation and polymerization. Complexation of Fe by HA may favor smaller particle sizes and inhibit aggregation, which is supported by the hydrodynamic diameter measurements described above. Cr(VI) reduction by Fe(II) can lead to Cr(III)−Fe(III) co-precipitates[72] and the initial nuclei formed presumably favor ferrihydrite over lepidocrocite.

The TEM images of Fe/Cr oxide precipitates formed from electrocoagulation shown in Figure 6 further confirm the role of HA in affecting the properties of EC solids. At pH 8 without humic acid, the precipitate exhibits a "hedgehog-like" morphology that is similar to lepidocrocite-rich precipitates formed under the conditions of Fe(II) oxidation by DO.[73] However, for the solids produced by electrocoagulation in the presence of 5 mg/L humic acid, the hedgehog-like morphology disappeared and the precipitates consist of smaller particles with a smoother surface aggregated into flocs, in line with previous results for amorphous Fe(III)−HA precipitates.[74] The TEM analyses further demonstrate the electrosteric stabilization effect from HA at pH 8. To further examine how HA affected the morphology of precipitated iron oxides, experiments with adsorption of 5 mg/L HA onto preformed electrocoagulation products at pH 8 created in the absence of HA were conducted, and the TEM images are shown in Figures 6c. The hedgehog-like morphology is clear when HA adsorbs to preformed solids, distinct from iron oxides that are simultaneously precipitated in the presence of HA. Although the EXAFS shows that lepidocrocite still accounts for 23% of the solids generated after EC with 5 mg/L HA at pH 8, the hedgehog-like morphology was not visible in TEM images of this solids, which is probably because the particles were too small or the lepidocrocite in these particular samples did not have that morphology. At pH 6 without HA, we still could observe the hedgehog-like morphology although it is less pronounced than at pH 8, consistent with the XRD and EXAFS spectroscopy results showing more ferrihydrite formation at pH 6. With 5 mg/L HA, the precipitates show greater aggregation but still contain features suggesting that some lepidocrocite is present (Figure 6e).[73,75]

XAFS spectroscopy was also used to characterize the speciation of Cr in the solids produced by electrocoagulation treatment of Cr(VI) solutions. XANES spectra show that these solids contain solely Cr(III), as indicated by the lack of a large, single pre-edge feature at ~5991 eV (Figure S5). All solids have similar XANES and EXAFS spectra (Figure 7), indicating that Cr speciation is largely unaffected by conditions in the electrocoagulation reactor. Comparison of the XANES and EXAFS spectra to those of Fe−Cr co-precipitates that have Fe/Cr ratios of 3:1 and 1:3 shows that the EC products closely resemble the 3:1 co-precipitates (Figure S6) . This is consistent with prior work that found that the products of Cr(VI) reduction by Fe(II) have an Fe/Cr ratio of 3:1 due to the reaction stoichiometry.[72,76]

To examine the coordination environment of Cr within the Fe oxide mineral structure, shell-by-shell fitting was performed on Cr K-edge EXAFS spectra of EC products (Figure S7). Sample spectra were well-fit with one Cr−O shell at 1.98 Å and

DOI: 10.1021/acs.est.7b00371
Environ. Sci. Technol. XXXX, XXX, XXX−XXX

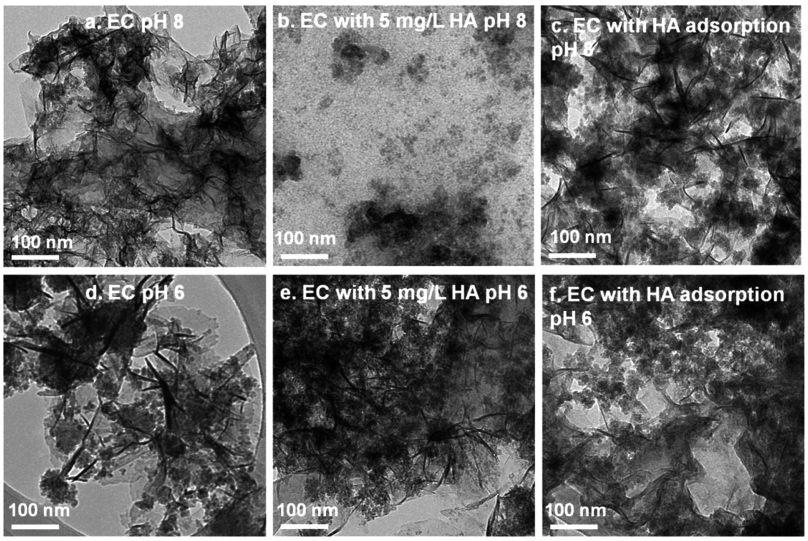

Figure 6. Transmission electron micrographs of solids produced by electrocoagulation at oxic conditions (a) at pH 8, (b) with 5 mg/L HA at pH 8, (c) at pH 8 and with postelectrocoagulation HA addition, (d) at pH 6, (e) with 5 mg/L HA at pH 6, (f) at pH 6 with postelectrocoagulation HA addition. Electrocoagulation with post HA addition was conducted by first producing solids in electrocoagulation and then adding HA 2 h later. Scale bar is 100 nm.

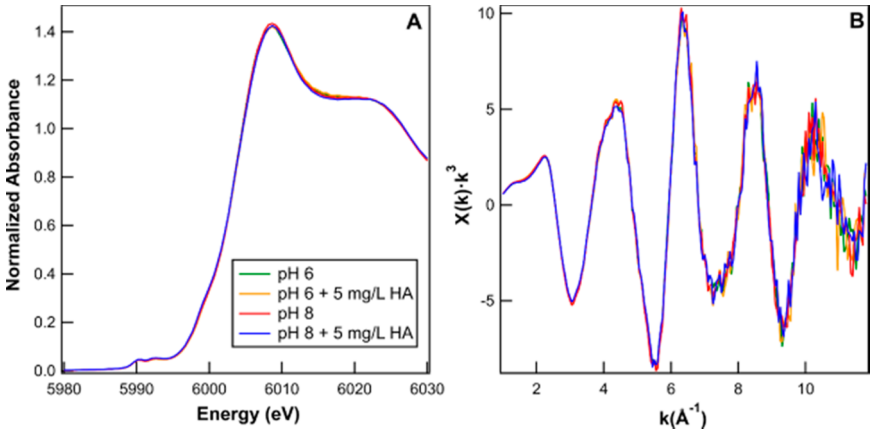

Figure 7. Cr K-edge (a) XANES and (b) EXAFS spectra of electrocoagulation products at pH 6 and pH 8 with and without 5 mg/L HA, all with an initial Cr(VI) concentration of 2 mg/L and operated at oxic conditions.

one Cr−Fe shell at 3.04 Å (Table S3). A second Cr−Fe shell could be fit at 3.5 Å or at 3.9 Å, but the *N* values for either fit refined to values within error of zero and increased the reduced χ^2 value making their addition not statistically justified. The lack of a second Cr−Fe shell, which was observed in prior studies of Cr−Fe co-precipitates,[72,77] may reflect the nanocrystalline nature of the products formed during electrocoagulation and the short reaction times (minutes) which inhibit particle ripening. The increase in ferrihydrite content upon addition of Cr(VI) during electrocoagulation suggests that in the present system Cr(VI) reduction by Fe(II) favors nucleation of ferrihydrite. Fitting also shows that HA does not alter Cr speciation, likely because ferrihydrite formation is also promoted during EC by HA.

Environmental Implications. Hexavalent chromium is a contaminant of great concern in water supplies, and iron-based electrocoagulation can effectively remove Cr(VI) to a very low concentration. The presence of humic acid in raw water during electrocoagulation leads to slower Cr(VI) removal at high pH, indicating that an electrocoagulation process will need more time to completely remove Cr(VI). The presence of HA also resulted in the formation of solid products with close association of Fe(III), Cr(III), and HA. The colloidal conditions of the electrocoagulation products would greatly influence the mobility of chromium even if all the Cr(VI) was reduced to Cr(III) by Fe(II) in EC. Cr(III), HA, and Fe(III) could pass through filtration steps when HA results in stable colloid formation during electrocoagulation at high pH. The passage of Cr(III) and HA through filtration steps as colloids could lead to concerns of Cr(III) reoxidation and DBP production during the later disinfection process in water treatment. Humic acid could be aggregated by optimizing the electrocoagulation operation conditions. (e.g., longer electrocoagulation time or higher dosage rate of Fe(II) from the anode with increasing the currency). All of the Cr in the solids produced by electrocoagulation was the less toxic Cr(III) form, and the coordination environment of Cr was indicative of Cr(III) incorporation into an iron oxide solid regardless of the presence of HA.

DOI: 10.1021/acs.est.7b00371
Environ. Sci. Technol. XXXX, XXX, XXX−XXX

■ ASSOCIATED CONTENT

Supporting Information

The Supporting Information is available free of charge on the ACS Publications website at DOI: 10.1021/acs.est.7b00371.

Additional information regarding Faraday's law, dynamic modeling, zeta potential of solids produced from EC, the concentration of colloidal Cr, HA, and Fe in EC, Cr XANES spectra, and Cr EXAFS fitting parameters (PDF)

■ AUTHOR INFORMATION

Corresponding Author

*Phone: (314) 935-6849; fax: (314) 935-7211; e-mail: giammar@wustl.edu.

ORCID

Peng Liao: 0000-0001-6924-1097
Jeffrey G. Catalano: 0000-0001-9311-977X
Wenlu Li: 0000-0003-3938-1624
Daniel E. Giammar: 0000-0002-4634-5640

Notes

The authors declare no competing financial interest.

■ ACKNOWLEDGMENTS

This research was supported by the U.S. National Science Foundation (CBET 1335613). C.P. acknowledges financial support from the School of Engineering Applied Science in Washington University in St. Louis for a first year Ph.D. fellowship. This research used resources of the Advanced Photon Source, a U.S. Department of Energy (DOE) Office of Science User Facility operated for the DOE Office of Science by Argonne National Laboratory under Contract No. DE-AC02-06CH11357. Walter Schenkeveld graciously provided pure lepidocrocite for XRD and EXAFS measurements and comparison with patterns of experimentally generated solids.

■ REFERENCES

(1) Qin, G.; McGuire, M. J.; Blute, N. K.; Seidel, C.; Fong, L. Hexavalent chromium removal by reduction with ferrous sulfate, coagulation, and filtration: A pilot-scale study. *Environ. Sci. Technol.* **2005**, *39* (16), 6321−6327.

(2) Brandhuber, P.; Frey, M.; McGuire, M. Low-level hexavalent chromium treatment options: bench-scale evaluation. *WaterRF Report No. 91042F*; Water Research Foundation: Denver, 2005.

(3) Eary, L. E.; Rai, D. Chromate removal from aqueous wastes by reduction with ferrous ion. *Environ. Sci. Technol.* **1988**, *22* (8), 972−977.

(4) Pan, C.; Troyer, L. D.; Catalano, J. G.; Giammar, D. E. Dynamics of chromium(VI) removal from drinking water by iron electrocoagulation. *Environ. Sci. Technol.* **2016**, *50* (24), 13502−13510.

(5) Kuokkanen, V.; Kuokkanen, T.; Rämö, J.; Lassi, U. Electrocoagulation treatment of peat bog drainage water containing humic substances. *Water Res.* **2015**, *79*, 79−87.

(6) Dubrawski, K. L.; Mohseni, M. In-situ identification of iron electrocoagulation speciation and application for natural organic matter (NOM) removal. *Water Res.* **2013**, *47* (14), 5371−5380.

(7) Aiken, G.; McKnight, D.; Wershaw, R.; MacCarthy, P. *Humic substances in soil, sediment, and water: geochemistry, isolation and characterization*; Wiley, 1985.

(8) Thurman, E. M.; Wershaw, R. L.; Malcolm, R. L.; Pinckney, D. J. Molecular size of aquatic humic substances. *Org. Geochem.* **1982**, *4* (1), 27−35.

(9) Tipping, E. *Cation binding by humic substances*. Cambridge University Press: Cambridge, United Kingdom. 2002.

(10) Wang, Y. G.; Michel, F. M.; Choi, Y.; Eng, P. J.; Levard, C.; Siebner, H.; Gu, B. H.; Bargar, J. R.; Brown, G. E. Pb, Cu, and Zn distributions at humic acid-coated metal-oxide surfaces. *Geochim. Cosmochim. Acta* **2016**, *188*, 407−423.

(11) Gledhill, M.; Buck, K. N. The organic complexation of iron in the marine environment: a review. *Front. Microbiol.* **2012**, *3*, 1−17.

(12) Tipping, E. Modeling ion-binding by humic acids. *Colloids Surf., A* **1993**, *73*, 117−131.

(13) Lalonde, K.; Mucci, A.; Ouellet, A.; Gélinas, Y. Preservation of organic matter in sediments promoted by iron. *Nature* **2012**, *483* (7388), 198−200.

(14) Tombácz, E.; Libor, Z.; Illés, E.; Majzik, A.; Klumpp, E. The role of reactive surface sites and complexation by humic acids in the interaction of clay mineral and iron oxide particles. *Org. Geochem.* **2004**, *35* (3), 257−267.

(15) Gu, B.; Schmitt, J.; Chen, Z.; Liang, L.; Mccarthy, J. F. Adsorption and desorption of natural organic matter on iron oxide: mechanisms and models. *Environ. Sci. Technol.* **1994**, *28* (1), 38−46.

(16) Illés, E.; Tombácz, E. The effect of humic acid adsorption on pH-dependent surface charging and aggregation of magnetite nanoparticles. *J. Colloid Interface Sci.* **2006**, *295* (1), 115−123.

(17) Chen, C.; Dynes, J. J.; Wang, J.; Sparks, D. L. Properties of Fe-Organic matter associations via co-precipitation versus adsorption. *Environ. Sci. Technol.* **2014**, *48* (23), 13751−13759.

(18) Mikutta, R.; Schaumann, G. E.; Gildemeister, D.; Bonneville, S.; Kramer, M. G.; Chorover, J.; Chadwick, O. A.; Guggenberger, G. Biogeochemistry of mineral−organic associations across a long-term mineralogical soil gradient (0.3−4100kyr), Hawaiian Islands. *Geochim. Cosmochim. Acta* **2009**, *73* (7), 2034−2060.

(19) Wagai, R.; Mayer, L. M. Sorptive stabilization of organic matter in soils by hydrous iron oxides. *Geochim. Cosmochim. Acta* **2007**, *71* (1), 25−35.

(20) Eusterhues, K.; Wagner, F. E.; Häusler, W.; Hanzlik, M.; Knicker, H.; Totsche, K. U.; Kögel-Knabner, I.; Schwertmann, U. Characterization of ferrihydrite-soil organic matter co-precipitates by X-ray diffraction and Mössbauer spectroscopy. *Environ. Sci. Technol.* **2008**, *42* (21), 7891−7897.

(21) Karlsson, T.; Persson, P. Coordination chemistry and hydrolysis of Fe(III) in a peat humic acid studied by X-ray absorption spectroscopy. *Geochim. Cosmochim. Acta* **2010**, *74* (1), 30−40.

(22) Benedetti, M. F.; Van Riemsdijk, W. H.; Koopal, L. K.; Kinniburgh, D. G.; Gooddy, D. C.; Milne, C. J. Metal ion binding by natural organic matter: From the model to the field. *Geochim. Cosmochim. Acta* **1996**, *60* (14), 2503−2513.

(23) Gustafsson, J. P.; Persson, I.; Oromieh, A. G.; van Schaik, J. W. J.; Sjöstedt, C.; Kleja, D. B. Chromium(III) complexation to natural organic matter: mechanisms and modeling. *Environ. Sci. Technol.* **2014**, *48* (3), 1753−1761.

(24) Westall, J. C.; Jones, J. D.; Turner, G. D.; Zachara, J. M. Models for association of metal ions with heterogeneous environmental sorbents. 1. complexation of Co(II) by leonardite humic acid as a function of pH and $NaClO_4$ concentration. *Environ. Sci. Technol.* **1995**, *29* (4), 951−959.

(25) Mak, M. S. H.; Lo, I. M. C. Influences of redox transformation, metal complexation and aggregation of fulvic acid and humic acid on Cr(VI) and As(V) removal by zero-valent iron. *Chemosphere* **2011**, *84* (2), 234−240.

(26) Liu, T.; Tsang, D. C.; Lo, I. M. Chromium(VI) reduction kinetics by zero-valent iron in moderately hard water with humic acid: iron dissolution and humic acid adsorption. *Environ. Sci. Technol.* **2008**, *42* (6), 2092−2098.

(27) Theis, T. L.; Singer, P. C. Complexation of iron(II) by organic matter and its effect on iron(II) oxygenation. *Environ. Sci. Technol.* **1974**, *8* (6), 569−573.

(28) Miles, C. J.; Brezonik, P. L. Oxygen consumption in humic-colored waters by a photochemical ferrous-ferric catalytic cycle. *Environ. Sci. Technol.* **1981**, *15* (9), 1089−1095.

(29) Rose, A. L.; Waite, T. D. Kinetic model for Fe(II) oxidation in seawater in the absence and presence of natural organic matter. *Environ. Sci. Technol.* **2002**, *36* (3), 433−444.

DOI: 10.1021/acs.est.7b00371
Environ. Sci. Technol. XXXX, XXX, XXX−XXX

(30) Rose, A. L.; Waite, T. D. Effect of dissolved natural organic matter on the kinetics of ferrous iron oxygenation in seawater. *Environ. Sci. Technol.* **2003**, *37* (21), 4877−4886.
(31) Stumm, W.; Morgan, J. *Aquatic Chemistry*; Wiley, 1981; 780 pp.
(32) Liang, L.; Mcnabb, J. A.; Paulk, J. M.; Gu, B.; Mccarthy, J. F. Kinetics of iron(II) oxygenation at low partial pressure of oxygen in the presence of natural organic matter. *Environ. Sci. Technol.* **1993**, *27* (9), 1864−1870.
(33) Emmenegger, L.; King, D. W.; Sigg, L.; Sulzberger, B. Oxidation kinetics of Fe(II) in a eutrophic Swiss lake. *Environ. Sci. Technol.* **1998**, *32* (19), 2990−2996.
(34) Guan, X.; Dong, H.; Ma, J. Influence of phosphate, humic acid and silicate on the transformation of chromate by Fe(II) under suboxic conditions. *Sep. Purif. Technol.* **2011**, *78* (3), 253−260.
(35) Buerge, I. J.; Hug, S. J. Influence of organic ligands on chromium(VI) reduction by iron(II). *Environ. Sci. Technol.* **1998**, *32* (14), 2092−2099.
(36) Agrawal, S. G.; Fimmen, R. L.; Chin, Y.-P. Reduction of Cr(VI) to Cr(III) by Fe(II) in the presence of fulvic acids and in lacustrine pore water. *Chem. Geol.* **2009**, *262* (3), 328−335.
(37) Good, N. E.; Winget, G. D.; Winter, W.; Connolly, T. N.; Izawa, S.; Singh, R. M. Hydrogen ion buffers for biological research. *Biochemistry* **1966**, *5* (2), 467−477.
(38) Ferguson, W. J.; Braunschweiger, K.; Braunschweiger, W.; Smith, J. R.; McCormick, J. J.; Wasmann, C. C.; Jarvis, N. P.; Bell, D. H.; Good, N. E. Hydrogen ion buffers for biological research. *Anal. Biochem.* **1980**, *104* (2), 300−310.
(39) Hinkle, M. A.; Wang, Z.; Giammar, D. E.; Catalano, J. G. Interaction of Fe(II) with phosphate and sulfate on iron oxide surfaces. *Geochim. Cosmochim. Acta* **2015**, *158*, 130−146.
(40) Wang, Z.; Tebo, B. M.; Giammar, D. E. Effects of Mn(II) on UO_2 dissolution under anoxic and oxic conditions. *Environ. Sci. Technol.* **2014**, *48* (10), 5546−5554.
(41) Kim, C.; Zhou, Q.; Deng, B.; Thornton, E. C.; Xu, H. Chromium(VI) reduction by hydrogen sulfide in aqueous media: stoichiometry and kinetics. *Environ. Sci. Technol.* **2001**, *35* (11), 2219−2225.
(42) Buerge, I. J.; Hug, S. J. Kinetics and pH dependence of chromium(VI) reduction by iron(II). *Environ. Sci. Technol.* **1997**, *31* (5), 1426−1432.
(43) Carbonaro, R. F.; Gray, B. N.; Whitehead, C. F.; Stone, A. T. Carboxylate-containing chelating agent interactions with amorphous chromium hydroxide: adsorption and dissolution. *Geochim. Cosmochim. Acta* **2008**, *72* (13), 3241−3257.
(44) Lipson, D. A.; Raab, T. K.; Goria, D.; Zlamal, J. The contribution of Fe(III) and humic acid reduction to ecosystem respiration in drained thaw lake basins of the Arctic Coastal Plain. *Global Biogeochem. Cycles* **2013**, *27* (2), 399−409.
(45) Li, T.; Jiang, Y.; An, X.; Liu, H.; Hu, C.; Qu, J. Transformation of humic acid and halogenated byproduct formation in UV-chlorine processes. *Water Res.* **2016**, *102*, 421−427.
(46) Dries, J.; Bastiaens, L.; Springael, D.; Kuypers, S.; Agathos, S. N.; Diels, L. Effect of humic acids on heavy metal removal by zero-valent iron in batch and continuous flow column systems. *Water Res.* **2005**, *39* (15), 3531−3540.
(47) Jeon, B. H.; Burgos, W. D.; Royer, R. A.; Dempsey, B. A. Low-temperature oxygen trap for maintaining strict anoxic conditions. *J. Environ. Eng.* **2004**, *130* (11), 1407−1410.
(48) *SW-846 Test Method 7196A, Chromium, Hexavalent (Colorimetric)*; US EPA, 1992.
(49) Viollier, E.; Inglett, P. W.; Hunter, K.; Roychoudhury, A. N.; Van Cappellen, P. The ferrozine method revisited: Fe(II)/Fe(III) determination in natural waters. *Appl. Geochem.* **2000**, *15* (6), 785−790.
(50) Doane, T. A.; Horwáth, W. R. Eliminating interference from iron(III) for ultraviolet absorbance measurements of dissolved organic matter. *Chemosphere* **2010**, *78* (11), 1409−15.
(51) Luo, Y.; Giammar, D. E.; Huhmann, B. L.; Catalano, J. G. Speciation of selenium, arsenic, and zinc in class C fly ash. *Energy Fuels* **2011**, *25*, 2980−2987.
(52) Catalano, J. G.; Huhmann, B. L.; Luo, Y.; Mitnick, E. H.; Slavney, A.; Giammar, D. E. Metal release and speciation changes during wet aging of coal fly ashes. *Environ. Sci. Technol.* **2012**, *46* (21), 11804−11812.
(53) Schwertmann, U.; Cornell, R. M. *Iron oxides in the laboratory: preparation and characterization*; John Wiley & Sons, 2008.
(54) Ravel, B.; Newville, M. ATHENA, ARTEMIS, HEPHAESTUS: data analysis for X-ray absorption spectroscopy using IFEFFIT. *J. Synchrotron Radiat.* **2005**, *12*, 537−541.
(55) Newville, M. IFEFFIT: interactive XAFS analysis and FEFF fitting. *J. Synchrotron Radiat.* **2001**, *8* (2), 322−324.
(56) Webb, S. M. SIXPack: A graphical user interface for XAS analysis using IFEFFIT. *Phys. Scr.* **2005**, *T115*, 1011−1014.
(57) Ankudinov, A. L.; Rehr, J. J. Relativistic calculations of spin-dependent x-ray-absorption spectra. *Phys. Rev. B: Condens. Matter Mater. Phys.* **1997**, *56* (4), R1712−R1715.
(58) Nagai, T.; Kagi, H.; Yamanaka, T. Variation of hydrogen bonded O···O distances in goethite at high pressure. *Am. Mineral.* **2003**, *88* (10), 1423−1427.
(59) Voelker, B. M.; Sulzberger, B. Effects of fulvic acid on Fe(II) oxidation by hydrogen peroxide. *Environ. Sci. Technol.* **1996**, *30* (4), 1106−1114.
(60) Wang, Z.; Schenkeveld, W. D.; Kraemer, S. M.; Giammar, D. E. Synergistic effect of reductive and ligand-promoted dissolution of goethite. *Environ. Sci. Technol.* **2015**, *49* (12), 7236−7244.
(61) Kim, D.; Duckworth, O. W.; Strathmann, T. J. Reactions of aqueous iron−DFOB (desferrioxamine B) complexes with flavin mononucleotide in the absence of strong iron(II) chelators. *Geochim. Cosmochim. Acta* **2010**, *74* (5), 1513−1529.
(62) Wan, W.; Pepping, T. J.; Banerji, T.; Chaudhari, S.; Giammar, D. E. Effects of water chemistry on arsenic removal from drinking water by electrocoagulation. *Water Res.* **2011**, *45* (1), 384−392.
(63) Liao, P.; Li, W.; Wang, D.; Jiang, Y.; Pan, C.; Fortner, J. D.; Yuan, S. Effect of reduced humic acid on the transport of ferrihydrite nanoparticles under anoxic conditions. *Water Res.* **2017**, *109*, 347−357.
(64) Yan, S. C.; Ouyang, S. X.; Gao, J.; Yang, M.; Feng, J. Y.; Fan, X. X.; Wan, L. J.; Li, Z. S.; Ye, J. H.; Zhou, Y. A room-temperature reactive-template route to mesoporous $ZnGa_2O_4$ with improved photocatalytic activity in reduction of CO_2. *Angew. Chem.* **2010**, *122* (36), 6544−6548.
(65) Xie, Y. *Disinfection byproducts in drinking water: Formation, analysis, and control*; CRC Press, 2016.
(66) Diemert, S.; Wang, W.; Andrews, R. C.; Li, X.-F. Removal of halo-benzoquinone (emerging disinfection by-product) precursor material from three surface waters using coagulation. *Water Res.* **2013**, *47* (5), 1773−1782.
(67) Watson, K.; Farré, M. J.; Knight, N. Enhanced coagulation with powdered activated carbon or MIEX® secondary treatment: a comparison of disinfection by-product formation and precursor removal. *Water Res.* **2015**, *68*, 454−466.
(68) Tian, C.; Liu, R.; Liu, H.; Qu, J. Disinfection by-products formation and precursors transformation during chlorination and chloramination of highly-polluted source water: Significance of ammonia. *Water Res.* **2013**, *47* (15), 5901−5910.
(69) Dubrawski, K. L.; Mohseni, M. Standardizing electrocoagulation reactor design: Iron electrodes for NOM removal. *Chemosphere* **2013**, *91* (1), 55−60.
(70) Rodrigues, A.; Brito, A.; Janknecht, P.; Proença, M. F.; Nogueira, R. Quantification of humic acids in surface water: effects of divalent cations, pH, and filtration. *J. Environ. Monit.* **2009**, *11* (2), 377−382.
(71) Liu, T. Z.; Rao, P. H.; Lo, I. M. C. Influences of humic acid, bicarbonate and calcium on Cr(VI) reductive removal by zero-valent iron. *Sci. Total Environ.* **2009**, *407* (10), 3407−3414.

DOI: 10.1021/acs.est.7b00371
Environ. Sci. Technol. XXXX, XXX, XXX−XXX

(72) Hansel, C. M.; Wielinga, B. W.; Fendorf, S. Structural and compositional evolution of Cr/Fe solids after indirect chromate reduction by dissimilatory iron-reducing bacteria. *Geochim. Cosmochim. Acta* **2003**, *67* (3), 401−412.
(73) Voegelin, A.; Senn, A. C.; Kaegi, R.; Hug, S. J.; Mangold, S. Dynamic Fe-precipitate formation induced by Fe(II) oxidation in aerated phosphate-containing water. *Geochim. Cosmochim. Acta* **2013**, *117* (5), 216−231.
(74) Schwertmann, U.; Wagner, F.; Knicker, H. Ferrihydrite−humic associations. *Soil Sci. Soc. Am. J.* **2005**, *69* (4), 1009−1015.
(75) Song, J.; Jia, S. Y.; Yu, B.; Wu, S. H.; Han, X. Formation of iron (hydr)oxides during the abiotic oxidation of Fe(II) in the presence of arsenate. *J. Hazard. Mater.* **2015**, *294*, 70−79.
(76) Papassiopi, N.; Pinakidou, F.; Katsikini, M.; Antipas, G. S. E.; Christou, C.; Xenidis, A.; Paloura, E. C. A XAFS study of plain and composite iron(III) and chromium(III) hydroxides. *Chemosphere* **2014**, *111*, 169−176.
(77) Charlet, L.; Manceau, A. A. X-ray absorption spectroscopic study of the sorption of Cr(III) at the oxide-water interface: II. Adsorption, co-precipitation, and surface precipitation on hydrous ferric oxide. *J. Colloid Interface Sci.* **1992**, *148* (2), 443−458.

DOI: 10.1021/acs.est.7b00371
Environ. Sci. Technol. XXXX, XXX, XXX−XXX